JOURNAL OF SOLID STATE CHEMISTRY 39, 395–400 (1981)

Preparation and Properties of the System $Fe_{1-x}Cr_xNbO_4$

B. KHAZAI, R. KERSHAW, K. DWIGHT, AND A. WOLD*

Department of Chemistry, Brown University, Providence, Rhode Island 02912

Received March 9, 1981; in final form May 26, 1981

Members of the system $Fe_{1-x}Cr_xNbO_4$ were prepared and their magnetic and electronic properties were investigated. It was shown that chromium substitution favored the formation of the rutile structure, which resulted in a decrease in the electrical conductivity because of randomization of the transition metal ions in the structure. The replacement of a few percent of Fe^{3+} with Cr^{3+} caused a significant lowering of the lowest optical band gap, whereas the higher-energy transitions remained essentially unchanged. This resulted in increased response to the longer wavelengths of the solar spectrum.

Introduction

The binary oxide of niobium, Nb_2O_5, has been reported to have an optical band gap of 3.4 eV (*1*). This would suggest that such a material, when used as an *n*-type photoanode for the photoassisted decomposition of water, would be limited in its absorptivity to the ultraviolet region of the spectrum ($\lambda < 400$ nm). In $Sr_2Nb_2O_7$, where NbO_6 octahedra are the photoactive centers, the material shows a band gap of 3.86 eV without any significant absorption of the visible radiation (*2*). However, it has been shown that the association of Fe_2O_3, band gap 2.2 eV (*3*), with Nb_2O_5 in $FeNbO_4$ results in enhancement of quantum efficiency, as well as extension of absorption to longer wavelengths (*4*). It has also been reported recently (*5*) that Cr^{3+}-doped TiO_2 shows photocurrents resulting from low-energy electronic excitations, which would indicate a lowering of the optical band gap. Such an observation, along with the low band gap of Cr_2O_3, 1.4 eV (*6*), would suggest the use of chromium as a possible dopant in order to produce more efficient photoanodes.

It was indicated in an earlier publication (*4*) that $FeNbO_4$ can form a solid solution with $FeNb_2O_6$, which would give rise to a conducting oxide. Such a compound, where the different valencies of the transition metal ion are located at identical lattice sites, should also show interesting magnetic properties resulting from interaction of 3*d* electrons. In this study, the effect of the substitution of chromium for iron on the electronic and magnetic properties of $FeNbO_4$ will be reported.

Experimental

Synthesis

All materials were prepared from the solid-state reaction between Fe_2O_3 (Johnson–Matthey, spec. pure), Nb_2O_5 (Kawecki Berylco Industries, spectroscopic grade), and Cr_2O_3 which was obtained by the care-

* To whom all correspondence should be addressed.

0022-4596/81/120395-06$02.00/0

ful thermal decomposition of ammonium dichromate (Allied Chemical Co.). Iron niobate, as well as the chromium-substituted samples, was prepared by placing a finely ground mixture of appropriate amounts of the starting materials in a platinum crucible and heating in air at 1150°C for 48 hr. Each sample was X-rayed and then reheated. After a third heating, the product was cooled to room temperature in the furnace and reexamined by X-ray analysis. This was done in order to confirm the formation of a single phase. A Philips Norelco diffractometer, with Cu$K\alpha$ radiation (1.5405 Å) at a scan rate of 0.25° 2θ/min, was used.

Disks were formed by pressing aliquots of approximately 150 mg at 90,000 psi; five drops of Carbowax were added to the powder before pressing, in order to facilitate the formation of a well-sintered disk. The pressed disks were placed on a bed of powder having the same composition in an alumina crucible. The disks were heated in a hollow globar furnace at a rate of 85°/hr to 1250°C and maintained at that temperature for 24 hr. At the end of the sintering process, the disks were cooled at the same rate.

X-Ray diffraction patterns of the sintered disks showed, at the limit of detection, the presence of the strongest line of α-Fe_2O_3, which is consistent with the formation of a solid solution of $FeNb_2O_6$ in $FeNbO_4$ under the sintering conditions. Essentially identical resistivities were measured before and after abrading these disks to one-half their original thickness, establishing their homogeneity.

Magnetic Measurements

Magnetic susceptibilities were measured using a Faraday balance (*7*) over the range from liquid nitrogen to room temperature at a field strength of 10.4 kOe. Honda–Owen (field dependency) plots were also made to determine the presence or absence of ferromagnetic impurities. The data were then corrected for core diamagnetism (*8*).

Electrical Measurements

The resistivities of the samples were measured using the Van der Pauw technique (*9*). Contacts were made by the ultrasonic soldering of indium directly onto the samples, and their ohmic behavior was established by measuring their current–voltage characteristics.

Electrode Preparation

Photoanodes were prepared by evaporating thin films of gold on the backs of the disks to provide good electrical contact. The gold face of each disk was attached to the electrode by means of indium solder. Miccrostop (Michigan Chrome Chemical Corp.) was applied to the gold face and the electrode wire for insulation. The photoelectrolysis measurements were carried out with a 150-W xenon lamp, a monochromator (Oriel Model 7240), a glass cell with a quartz window, and a current amplifier as described previously (*10*). The electrolyte, 0.2 *M* sodium acetate (pH = 7.8), was purged of dissolved oxygen by continuous bubbling of 85% argon–15% hydrogen gas.

Structure

$FeNbO_4$ has been reported to crystallize with the monoclinic wolframite structure (space group $P2/C$) below 1085°C. Roth (*11*) and Laves (*12*) have shown that between 1085 and 1380°C, a transition to the orthorhombic α-PbO_2 structure (space group *Pbcn*) occurs, followed by a further transformation to the tetragonal rutile structure (space group $P4_2/mnm$) above 1380°C.

In the rutile form of $FeNbO_4$, shown in Fig. 1a, it can be seen that the octahedra share edges in such a way that straight chains are formed along the c direction (perpendicular to the plane of the paper). As shown in Fig. 1b, there is a random

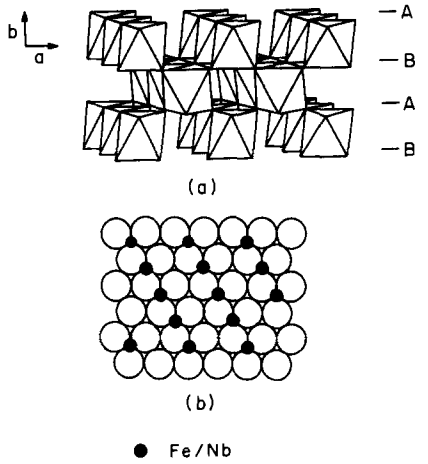

FIG. 1. The structure of rutile, MO_2: (a) packing of MO_6 octahedra; (b) closest-packed arrangement of oxygen around M atoms.

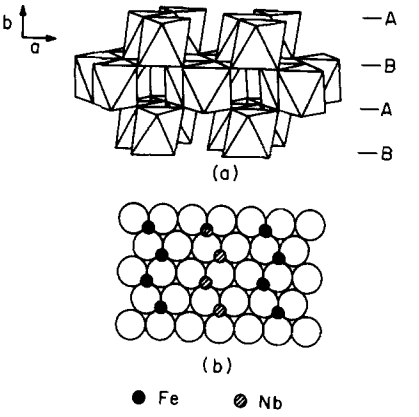

FIG. 3. Structure of wolframite $FeNbO_4$: (a) packing of MO_6 octahedra; (b) closest-packed layer of oxygen around Fe and Nb atoms.

distribution of Fe and Nb atoms in one-half of the available octahedral sites. On the other hand, when $FeNbO_4$ crystallizes with the α-PbO_2 structure, the MO_6 units are joined in such a way as to form zigzag chains of octahedra along the c direction (Fig. 2). As with the rutile structure, only one-half of the octahedral sites are occupied, and random distribution of Fe and Nb atoms in the zigzag chains prevails. The wolframite polymorph (Fig. 3) is an ordered variant of the α-PbO_2 structure in which the

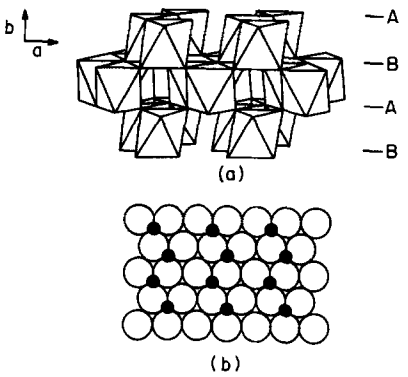

FIG. 2. The structure of α-PbO_2: (a) packing of MO_6 octahedra; (b) closest-packed arrangement of oxygen around M atoms.

Fe and Nb atoms are distributed in such a fashion that every occupied chain contains either only Fe or only Nb atoms. The transformation of wolframite to α-PbO_2, which occurs at elevated temperatures, is therefore considered to be the result of randomization of Fe and Nb atoms within the structural array.

Thus, for $FeNbO_4$, the rutile and α-PbO_2 are related to the nature of the chains formed, i.e., straight or zigzag. In both polymorphs, the Fe and Nb atoms are arranged in a random fashion. Ordering of the atoms has been observed in the zigzag chains, and such ordering gives rise to the formation of the wolframite structure.

Results

The system $Fe_{1-x}Cr_xNbO_4$ forms a solid solution crystallizing with the wolframite structure over a composition range of $0 < x < 0.1$. In the region $0.1 < x < 0.4$, a mixture of the wolframite $FeNbO_4$ and rutile $CrNbO_4$ phases was obtained. Between $0.4 \leq x \leq 1$, the products can be indexed on the basis of the rutile $CrNbO_4$ structure. The precision lattice parameters are listed in Table I. The changes in the cell parameters may be attributed to the difference in the ionic radii of Fe^{3+} (0.65 Å) and Cr^{3+} (0.615

TABLE I

PRECISION LATTICE CONSTANTS FOR THE SYSTEM $Fe_{1-x}Cr_xNbO_4$

	a (Å)	b (Å)	c (Å)	β (deg)
$FeNbO_4$	4.997(2)	5.619(2)	4.651(2)	90
$Fe_{0.9}Cr_{0.1}NbO_4$	4.996(2)	5.611(2)	4.642(2)	89.79
$Fe_{0.6}Cr_{0.4}NbO_4$	4.670(2)	—	3.030(2)	—
$CrNbO_4$	4.645(2)	—	3.012(2)	—

Å). Table II indicates the change in the electrical resistivities in going from the wolframite compositions to those of the rutile. The electrical resistivity is enhanced greatly as the structure is transformed from wolframite to rutile. The resistivity varies from 53 ohm-cm for $x = 0.1$ (wolframite) to an insulator for $x = 0.4$ (rutile). Such a difference can be explained in terms of the ordering of iron and niobium chains in the wolframite structure. As indicated previously (*4*), $FeNbO_4$ can form a solid solution with $FeNb_2O_6$. Cation ordering of the zigzag chains prevents the Nb^{5+} ions from blocking the conduction paths which result from the coexistence of Fe^{2+} and Fe^{3+} ions in the alternate chains (Fig. 3). This gives rise to the observed increase in conductivity. For products which crystallize with the straight-chain rutile structure, there is a lack of ordering of the FeO_6 and NbO_6 octahedra, and hence, low electrical conductivity is observed.

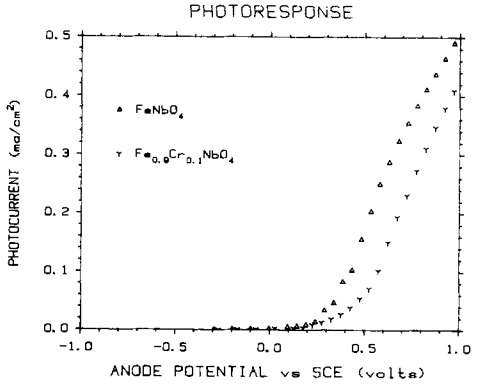

FIG. 4. Variation of photocurrent with anode potential under "white" xenon arc irradiation of 1.0 W/cm² in 0.2 *M* sodium acetate adjusted to pH = 7.8.

The magnetic data for the system $Fe_{1-x}Cr_xNbO_4$ is summarized in Table II. All compositions show Curie–Weiss behavior with effective molar Curie constants, C_M, corresponding to those expected from spin-only moment considerations involving primarily Fe^{3+}, Cr^{3+}, and Nb^{5+}. A high spin state for both Fe^{3+} and Cr^{3+} ($\mu_{eff}Nb^{5+} = 0$) is assumed. From Table II, it can be seen that the value of the paramagnetic Curie temperature, Θ, is negative and decreases in magnitude with increasing chromium substitution. The decrease in the Θ values given in Table II is attributed to a decrease in the strength of the antiferromagnetic interactions, caused by the substitution of d^3 chromium for d^5 iron.

The photoresponse observed for the

TABLE II

MAGNETIC AND ELECTRICAL DATA ON THE SYSTEM $Fe_{1-x}Cr_xNbO_4$

	Structure[a]	C_M(exp)	C_M(theo)	θ	ρ (ohms)
$FeNbO_4$	W	4.18	4.35	−79.8	40(1)
$Fe_{0.9}Cr_{0.1}NbO_4$	W	3.80	3.94[b]	−52.6	53(1)
$CrNbO_4$	R	1.87	1.87	−33.9	insul.

[a] W = wolframite; R = rutile.
[b] Corrected for $C_M(Fe^{3+}) = 4.18$.

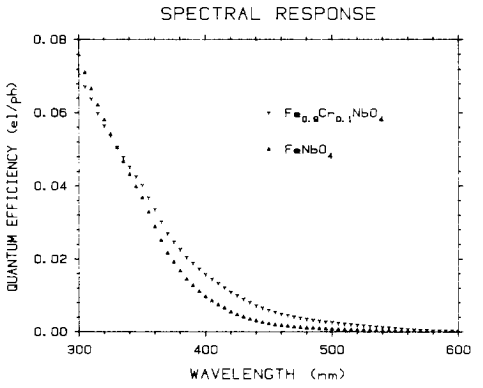

FIG. 5. Spectral variation of the quantum efficiency obtained at an anode potential of 0.8 V vs SCE in 0.2 *M* sodium acetate adjusted to pH = 7.8.

chromium-doped $FeNbO_4$ is represented in Fig. 4, where the photocurrents obtained in the "white" light are plotted against the anode potential measured with respect to a standard calomel electrode (SCE). The photoresponse curve for $FeNbO_4$ (*4*) is included for comparison. The general shapes of the two curves are quite similar. Although the onset of photocurrent is not sufficiently abrupt for an exact comparison of the flat-band potentials, there does not appear to be a significant shift, and as can be seen, the flat-band potential seems to lie between 0.1 and 0.4 V vs SCE for both compounds.

The quantum efficiency η (in electrons/photon) of $Fe_{0.9}Cr_{0.1}NbO_4$, as measured at an anode potential of 0.8 V vs SCE, is plotted in Fig. 5. Results for $FeNbO_4$ are again included for the purpose of comparison. Although the shapes of the spectral response curves remain similar, the photoresponse of the chromium-doped sample extends to longer wavelengths and possesses higher efficiency in the visible part of the spectrum. This increase in efficiency is sufficient to nearly double the total photoresponse to AM1 (air mass 1) solar irradiation, as can be seen from Fig. 6. Such an extension to longer wavelengths was also observed for the chromium-substituted systems $Ti_{1-x}Cr_xO_2$ and $BaTi_{1-x}Cr_xO_3$ (*5, 13, 14*). Unfortunately, further improvement of the photoresponse at higher wavelengths for chromium-substituted $FeNbO_4$ could not be achieved because of the high resistivity of the rutile phases. Even if these materials could be made conducting, they still would not be practical anodes for photoelectrolysis because of the high bias required by the observed flat-band potential.

Analysis of the spectral response data can yield values for the various energy transitions (*15*). Accordingly, the quantity $(nh\nu)^{0.5}$ is plotted as a function of the pho-

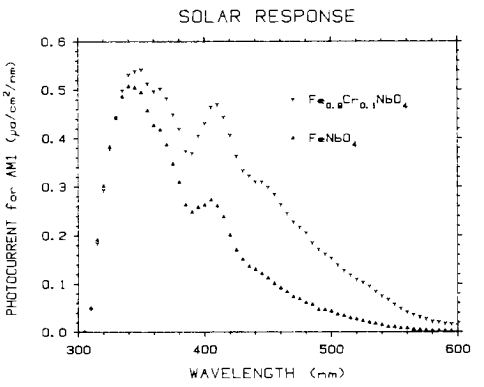

FIG. 6. Solar response for air mass 1 (AM1) calculated from the data presented in Fig. 5.

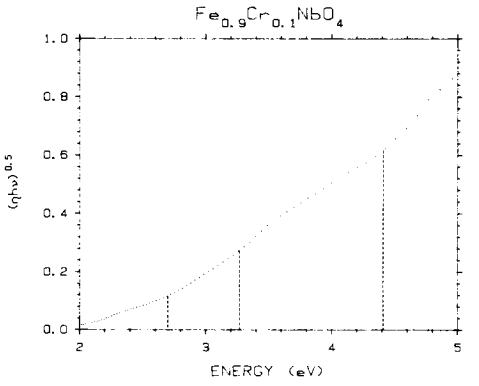

FIG. 7. Indirect band gap analysis for $Fe_{0.9}Cr_{0.1}NbO_4$, showing transitions at 1.90(5), 2.7(1), 3.27(3), and 4.41(2) eV.

ton energy in Fig. 7. This analysis yields a lowest-energy optical band gap of 1.90(5) eV. As previously reported, $FeNbO_4$ shows a lowest-energy transition of 2.08 eV. Consequently, there appears to be a significant lowering of the band gap on substitution of small amounts of chromium into $FeNbO_4$. This is in good agreement with the reported decrease in the optical band gap of α-Fe_2O_3 for a 10 mole% substitution of chromium (*16*). In addition, from the data presented in Fig. 7, several additional band transitions at higher energies can be estimated. These are indicated by sudden increases in the slope, such as occur at 2.7(1), 3.27(3), and 4.41(2) eV. The latter three energy gaps agree quite closely with the values of 2.68(2), 3.24(4), and 4.38(2) eV reported for pure $FeNbO_4$. Such an agreement suggests that the individual characteristics of the FeO_6 and NbO_6 centers of $FeNbO_4$ are not altered. The lowering of the optical band gap can, therefore, be attributed to the formation of Cr^{3+} ($3d^3$) energy levels within the optical band gap of $FeNbO_4$. However, as suggested by Goodenough (*14*) and Campet (*5*), some surface delocalization of $Cr^{3+}(3d^3)$ states are probably required to make the observed contributions to photoactivity possible.

Acknowledgments

The Office of Naval Research, Arlington, Virginia, supported the work of Bijan Khazai and Kirby Dwight. In addition, the authors would like to acknowledge the support of the Materials Research Laboratory Program at Brown University.

References

1. P. Clechet, J. Martin, R. Oliver, and C. Vallouy, *C. R. Acad. Sci. Paris Ser. C* **282**, 887 (1976).
2. J. Hormadaly, S. N. Subbarao, R. Kershaw, K. Dwight, and A. Wold, *J. Solid State Chem.* 33, 27 (1980).
3. W. H. Strehlow and E. L. Cook, *J. Phys. Chem. Ref. Data* **2**, 163 (1973).
4. J. Koenitzer, B. Khazai, J. Hormadaly, R. Kershaw, K. Dwight, and A. Wold, *J. Solid State Chem.* 35, 128 (1980).
5. G. Campet, J. Verniolle, J. P. Doumec, and J. Claverie, *Mater. Res. Bull.* **15**, 1135 (1980).
6. H. P. Maruska and A. Ghosh, *Solar Energy* **20**, 443 (1978).
7. B. Morris and A. Wold, *Rev. Sci. Instrum.* **39**, 1937 (1968).
8. P. W. Selwood, "Magnetochemistry," 2nd ed. Interscience, New York (1956).
9. L. J. Van der Pauw, *Philips Res. Rep.* **13**, 1 (1958).
10. S. N. Subbarao, Y. H. Yun, R. Kershaw, K. Dwight, and A. Wold, *Inorg. Chem.* **18**, 488 (1979).
11. R. S. Roth and J. Waring, *Amer. Mineral.* **49**, 243 (1964).
12. Von F. Laves, G. Bayer, and A. Panagos, *Schweiz. Mineral. Petrog. Mitt.* **43**, 217 (1963).
13. A. Monnier and J. Augustinski, *J. Electrochem. Soc.* **127**(7), 1576 (1980).
14. G. Campet, M. P. Dare-Edwards, A. Hammett, and J. B. Goodenough, *Nouv. J. Chem.* 4(819), 501 (1980).
15. F. P. Koffyberg, K. Dwight, and A. Wold, *Solid State Commun.* **30**, 433 (1979).
16. P. Merchant, R. Collins, R. Kershaw, K. Dwight, and A. Wold, *J. Solid State Chem.* **27**, 307 (1979).